U.S. DEPARTMENT OF ENERGY | Office of Science

DOE/SC-ARM-16-017

Characterization of Black Carbon Mixing State Field Campaign Report

A Sedlacek
P Davidovits
ER Lewis
TB Onasch

April 2016

ARM
CLIMATE RESEARCH FACILITY

DISCLAIMER

DOE/SC-ARM-16-017

Characterization of Black Carbon Mixing State Field Campaign Report

A Sedlacek, Brookhaven National Laboratory
Principal Investigator

P Davidovits, Boston College
ER Lewis, Brookhaven National Laboratory
TB Onasch, Aerodyne Research
Co-Investigators

April 2016

Work supported by the U.S. Department of Energy,
Office of Science, Office of Biological and Environmental Research

Executive Summary

Interpreting the temporal relationship between the scattering and incandescence signals recorded by the Single Particle Soot Photometer (SP2), Sedlacek et al. (2012) reported that 60% of the refractory black carbon containing particles in a plume containing biomass burning tracers exhibited non-core-shell structure. Because the relationship between the rBC (refractory black carbon) incandescence and the scattering signals had not been reported in the peer-reviewed literature, and to further evaluate the initial interpretation by Sedlacek et al., a series of experiments was undertaken to investigate black carbon-containing particles of known morphology using Regal black (RB), a proxy for collapsed soot, as the light-absorbing substance to characterize this signal relationship. Particles were formed by coagulation of RB with either a solid substance (sodium chloride or ammonium sulfate) or a liquid substance (dioctyl sebacate), and by condensation with dioctyl sebacate, the latter experiment forming particles in a core-shell configuration. Each particle type experienced fragmentation (observed as negative lagtimes), and each yielded similar lagtime responses in some instances, confounding attempts to differentiate particle morphology using current SP2 lagtime analysis. SP2 operating conditions, specifically laser power and sample flow rate, which in turn affect the particle heating and dissipation rates, play an important role in the behavior of particles in the SP2, including probability of fragmentation. This behavior also depended on the morphology of the particles and on the thermochemical properties of the non-RB substance. Although these influences cannot currently be unambiguously separated, the SP2 analysis may still provide useful information on particle mixing states and black carbon particle sources. This work was communicated in a 2015 publication (Sedlacek et al. 2015)

Acronyms and Abbreviations

ARI	Aerodyne Research, Inc.
ARM	Atmospheric Radiation Measurement Climate Research Facility
BC	black carbon
BC4	Boston College-Led Black Carbon Study 4
BNL	Brookhaven National Laboratory
DOE	U.S. Department of Energy
DOS	dioctyl sebacate
FWHM	full width at half maximum
nm	nanometer (10^{-9} m)
RB	Regal black (laboratory surrogate for black carbon)
rBC	refractory black carbon
SP2	Single Particle Soot Photometer

Contents

Figures

1.0 Background

The large uncertainty associated with black carbon (BC) direct forcing is due, in part, to the dependence of light absorption of BC-containing particles on the position of the BC within the particle. It is predicted that this absorption will be greatest for an idealized core-shell configuration in which the BC is a sphere at the center of the particle, whereas much less absorption should be observed for particles in which the BC is located near or on the surface (Fuller et al. 1999). Such microphysical information on BC-containing particles has previously been provided only by labor-intensive microscopy techniques, often requiring that climate modelers make assumptions about the location of the BC within the particle that are based more on mathematical simplicity than physical reality. A paper published by Sedlacek et al. (2012) interpreted the temporal behavior of the scattering and incandescence signals from individual particles containing refractory BC (rBC) measured by the Single Particle Soot Photometer (SP2) as rBC located near or at the surface as opposed to particle configurations that more closely resemble a core-shell configuration. In an effort to better characterize this "lagtime" analysis technique, a systematic series of laboratory experiments were carried out at Boston College.

Principal Investigators

Arthur J. Sedlacek III, Brookhaven National Laboratory

Co-Investigators

Paul Davidovits, Boston College
Ernie R. Lewis, Brookhaven National Laboratory
Timothy B. Onasch, Aerodyne Research

Additional Team Members

Andrew Lambe, Boston College

2.0 Notable Events or Highlights

Experiments were carried out during a 4-week laboratory campaign at Boston College. A new coagulation chamber, designed by Aerodyne Research, Inc. (ARI) and Boston College, was used in this study.

3.0 Lessons Learned

The difficulties encountered during the ARM-sponsored "SP2 at Boston College-Led Black Carbon (BC3) study" serve as a reminder of the need to allot enough time to fully characterize a new laboratory technique: in the present case, a particle coagulation chamber. While this characterization resulted in the BC3 not meeting its intended goal, the experiments carried out during BC3 set the stage for the successful follow-on campaign (BC4) and the subject of this final report.

4.0 Results

The reader is directed to Sedlacek and co-workers (2015) for a more detailed discussion of the results of this laboratory study. Below are selected highlights and a summary taken from that publication.

4.1 Experimental Details

In all experiments, atomized Regal black (RB, Cabot Corp.), which has a compact, aciniform solid structure, was used for the rBC component and was chosen as a surrogate for collapsed soot. Scattering and incandescence signals from individual particles were measured with an eight-channel SP2 (revision D). The mass of the rBC contained in a particle is determined from the peak magnitude of the incandescence signal by calibration with RB, and is reported as a mass-equivalent diameter ($D_{me, rBC}$) based on an assumed density of 1.8 g cm^3. The SP2 can detect incandescence signals from particles with $D_{me, rBC}$ in the range of ~70–600 nm, but scattering signals only from particles with initial diameters in the range of ~175–350 nm. The experimental setup is shown in Figure 1.

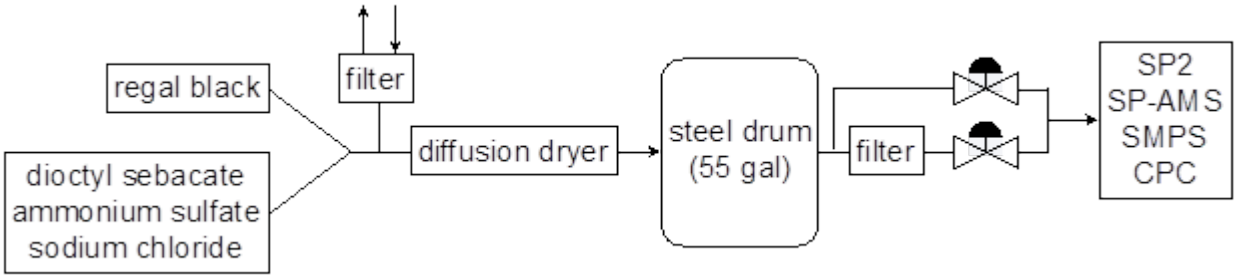

Figure 1. Experimental setup used to coagulate Regal black (RB) with sodium chloride (SC), ammonium sulfate (AS), and dioctyl sebacate (DOS). Not shown is the coating chamber used for RB→DOS coating experiments.

Regal black (RB) particles were (a) coagulated with drops of dioctyl sebacate (DOS, an organic substance that is liquid at room temperature) generated via homogenous nucleation in a heated flask, and (b) coated with DOS via gas-to-particle condensation, forming RB+DOS and DOS→RB particles, respectively. In the coagulation experiments, the techniques and sampling were the same as those used in the previous coagulation experiments with RB and sodium chloride (SC) or ammonium sulfate (AS). In the condensation experiments, the DOS→RB particles were formed by passing RB particles through a chamber with a heated bath containing DOS at various temperatures (103, 107, and 115 C); the dependence of vapor pressure on temperature resulted in different concentrations of DOS vapor and thus different coating thicknesses. The DOS→RB particles were sampled directly after leaving the chamber. This set of experiments was conducted to investigate the SP2 responses to particles formed by two different methods that may (at least initially) have different morphologies, i.e., DOS→RB particles are expected to have a core-shell configuration, whereas RB+DOS particles will not, at least initially.

However, the liquid DOS may wet RB and the coagulated particles may change morphologies (e.g., become more similar to core-shell) over time.

A final set of experiments investigated the dependence of lagtimes on SP2 operating conditions, specifically laser power (qualitatively indicated by laser diode current) and sample flow rate, both of which affect the heating rate of rBC-containing particles. Increasing the pump laser power results in increased intra-cavity laser intensity, and increasing the sample flow rate results in increased particle velocity, both of which lead to a greater rate of energy absorption by the rBC, less time for intra-particle heat transfer from the rBC to the non-rBC material, and thus increased particle heating rate.

4.2 Single-Particle SP2 Lagtime Measurements

Several types of single-particle SP2 scattering and incandescence signals were observed during this study, with varying frequency depending on the particle system studied. Examples for RB+SC and RB+DOS particles are shown in Figures 2a–g, respectively. In the first type (Figure 2a), the maximum of the scattering signal occurs before that of the incandescence signal, resulting in a positive lagtime. Under the core-shell assumption, this particle would be interpreted as having an rBC core with sufficient associated non-rBC material that it requires an appreciable time to absorb enough laser energy to evaporate this material. In the second type (Figure 2b), the maxima of the scattering and incandescence signals occur at nearly the same time, resulting in a lagtime of near zero. Such signals are interpreted as resulting from rBC-containing particles with little or no non-rBC material. In the third type (Figure 2c), the maximum of the scattering signal occurs after the peak of the incandescence signal, and thus results in a negative lagtime, behavior seemingly inconsistent with the conventional core-shell assumption. SP2 signals with two scattering peaks were also observed; for some of these (Figure 2d) the largest peak occurred before incandescence, whereas for others (Figure 2e) it occurred after incandescence. As the lagtime is defined as the time difference between the peak of the incandescence signal and the maximum value of the scattering signal (regardless of any other features of the scattering signal), these two situations correspond to positive and negative lagtime, respectively. For RB+DOS particles, two scattering peaks were also observed, with the smaller one occurring before incandescence and the larger one occurring either simultaneously with (Figure 2f) or after (Figure 2g) incandescence.

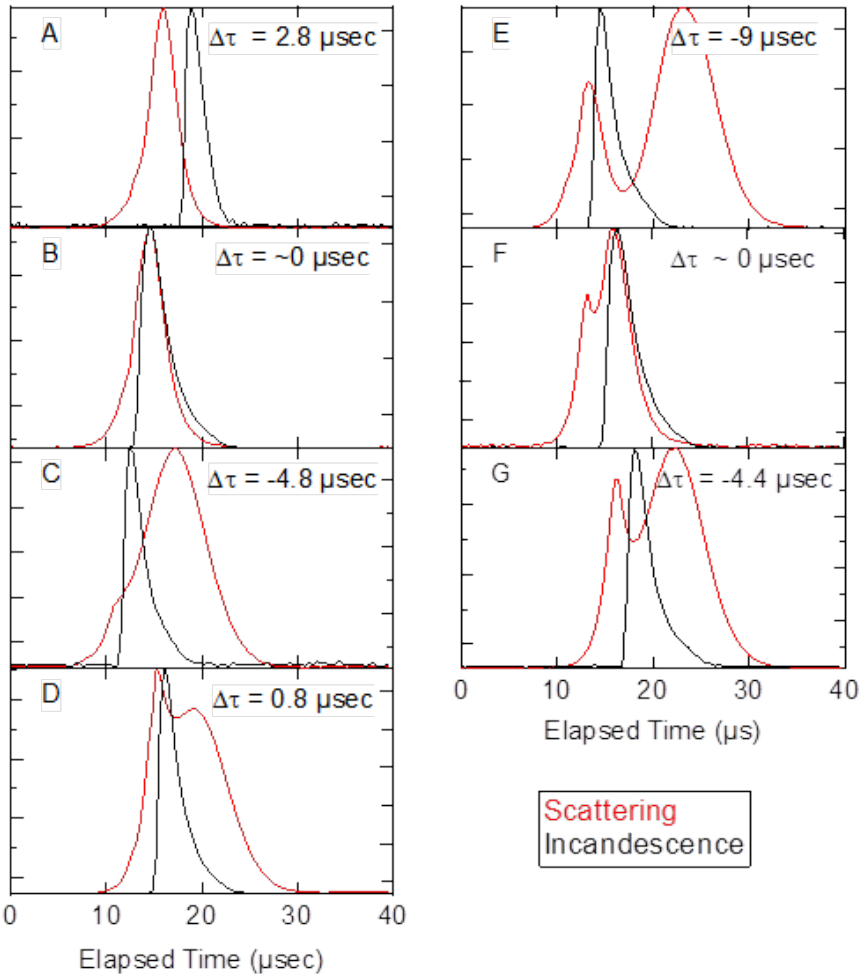

Figure 2. Examples of scattering and incandescence signals from individual RB+SC (a–e) and RB+DOS (f,g) particles: (a) scattering signal maximum occurs before incandescence signal maximum; (b) scattering signal maximum coincides with incandescence signal maximum; (c) scattering signal maximum occurs after incandescence signal maximum; (d) bimodal scattering signal with scattering signal maximum coincident with incandescence signal maximum and a second scattering peak after incandescence; (e) bimodal scattering signal with scattering signal maximum occurring after incandescence and a second scattering peak before incandescence; (f) bimodal scattering signal with scattering signal maximum coincident with incandescence signal maximum and a second scattering peak before incandescence; and (g) bimodal scattering signal with scattering signal maxima roughly equal in magnitude but opposite distance from the incandescence signal maximum.

4.3 Lagtime Distribution Plots

The distributions of lagtimes (derived from the time-dependent SP2 scattering and incandescence signals from individual particles) from each set of coagulation experiments (RB+SC, RB+AS, and RB+DOS) for short (<1 h), intermediate (1.5– 2 h), and long (>17 h) mixing times are plotted in Figure 3 as a function

of rBC mass-equivalent diameter, $D_{me, rBC}$. Colors represent the number fraction of particles within given ranges of Δt (400 ns) and $D_{me, rBC}$ (5 nm). In each case, the normalized size distribution of RB-number concentration in the representation $dN_{rBC}/d\log D_{me, rBC}$ is shown, as is the ratio of the number of particles with positive lagtimes to those with negative lagtimes (positive-to-negative lagtime ratio). Since positive and negative lagtimes only have meaning for rBC particles containing associated non-rBC material, this ratio excludes uncoated rBC particles. As the majority of RB particles remained uncoagulated with SC, AS, or DOS even at the longest mixing time, lagtimes of these particles are not included in the lagtime distribution figures. An RB particle was assumed to be uncoagulated if it had a value of Δt in the range -0.4 to 1.2 ms; this upper limit, although somewhat arbitrary, is commonly accepted in the SP2 research community and allows for uncertainties in instrument response. As particles resulting from coagulation between two or more RB particles will fall in this range, the lagtime distributions presented thus pertain only to particles resulting from coagulation of RB and non-rBC substance.

4.3.1 Coagulation of Regal Black and Sodium Chloride

Lagtime distributions for RB+SC particles are shown in the left column of Figure 3 as a function of $D_{me, rBC}$ for mixing times ranging from 0.6 h up to 17 h. All these distributions are qualitatively similar and have a prominent mode at small positive lagtimes (near ~1.5 ms) that extends to larger positive lagtimes at smaller values of $D_{me, rBC}$, and another mode at negative lagtimes that covers a wider range of values of Δt (from -1 to -3 ms). The location of the maximum value of $D_{me, rBC}$ for the mode at small positive lagtimes increases with increasing mixing time as a result of coagulation and gravitational settling processes. The most striking observation for the RB+SC system is the presence of both negative and positive lagtimes, which occur in roughly equal numbers (a positive- to-negative lagtime ratio of 0.7 implies that 41% of the lag- times are positive, and a positive-to-negative ratio of 1.2 implies that 54% of the lagtimes are positive). The occurrence of negative lagtimes is consistent with the original interpretation put forth by Sedlacek et al. (2012) that they originate from the rBC being located at or near the surface, but the presence of positive lagtimes is unexpected for the current situation of coagulated solid–solid particles.

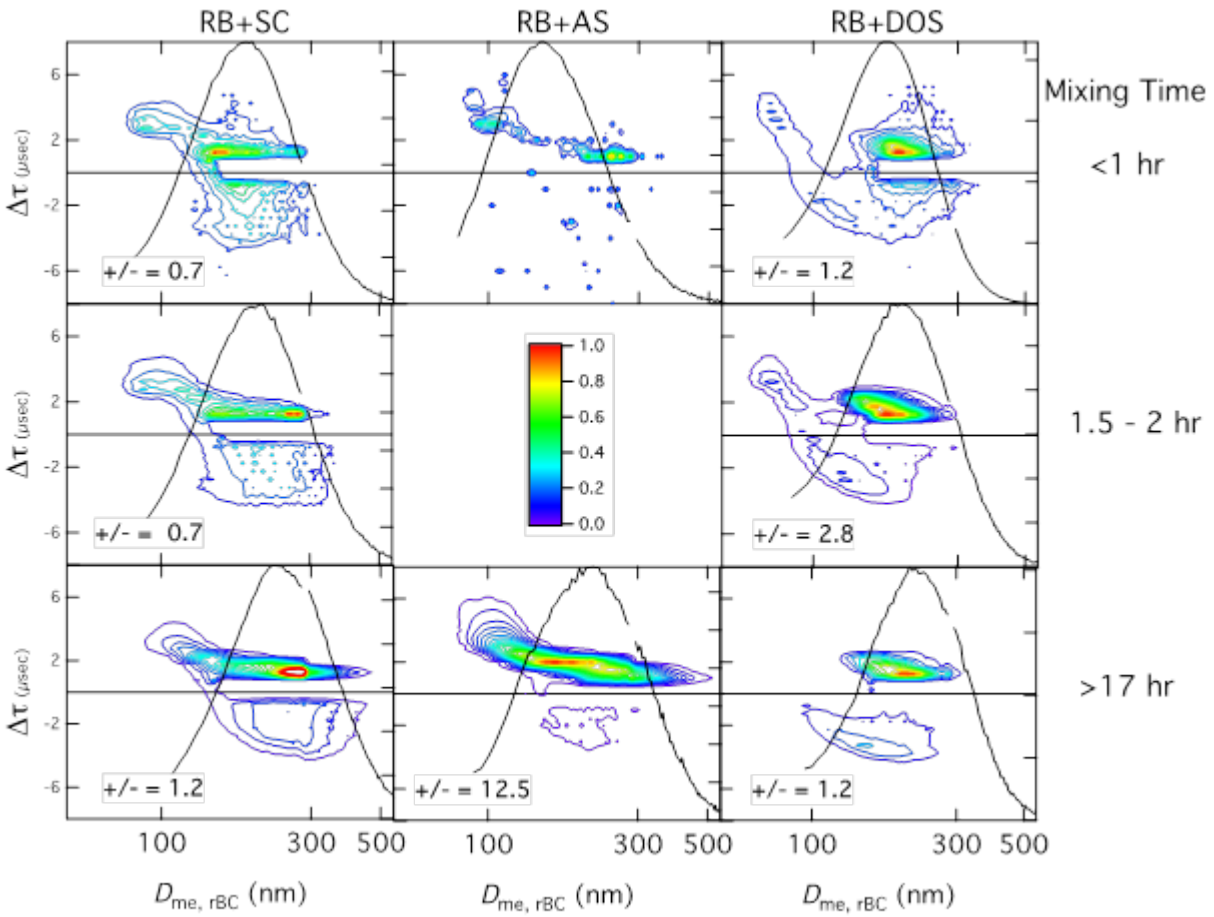

Figure 3. Lagtime distributions for RB+SC particles (left column), RB+AS particles (center column), and RBCDOS particles (right column) at different mixing times, determined by binning events in ranges of lagtime, Δt (400 ns) and rBC mass-equivalent diameter, $D_{me, rBC}$ (5 nm). Colors represent the number fraction of particles within given ranges of Δt and $D_{me, rBC}$. As the majority of RB particles remain uncoagulated, lagtimes of these particles are not included in the figures. Also shown are the normalized size distributions of RB-number concentration, $dN_{rBC}/dlogD_{me, rBC}$, and the positive-to-negative lagtime ratio (number of particles with positive lagtimes to those with negative lagtimes).

4.3.2 Coagulation of Regal Black and Ammonium Sulfate

Lagtime distributions for RB+AS particles for mixing times of 1 h and 20.6 h are shown in Figure 3 (middle column). At the shortest mixing times, there are fewer RB+AS coagulated particles than for RB+SC at the shortest mixing time (probably because of differences in the relative distributions of SC, AS, and RB for the different situations), and no positive-to-negative lagtime ratio is presented for this situation. At the longest mixing time, the RB+AS lagtime distribution is qualitatively similar to that for RB+SC at all mixing times and exhibits both positive and negative lagtimes, although the fraction of negative lagtimes for RB+AS particles is substantially smaller than that for RB+SC particles (the positive-to-negative lagtime ratio is 12.5 for RB+AS compared with 1.2 for RB+SC).

4.3.3 Coagulation of Regal Black and Dioctyl Sebacate

Lagtime distributions for RB+DOS particles (Figure 3, right column) also exhibit both negative and positive lagtimes. The distribution for the shortest mixing time is qualitatively similar to those for the RB+SC system at all mixing times (and to that for RB+AS at the longest mixing time); specifically, there is a dominant mode at positive lagtimes centered near 1.5 ms distributed over a range of values of $D_{me, rBC}$, and another, less prominent mode at negative lagtimes distributed over a wide range of lagtimes. In contrast to the RB+SC and RB+AS cases, however, the RB+DOS distribution at the longest mixing time looks qualitatively different and has a second negative lagtime mode centered near -3.4 ms and 150 nm. The RB+DOS lagtime distributions exhibit a greater change with increasing mixing time than do those for RB+SC or RB+AS; the secondary positive lagtime mode at small $D_{me, rBC}$ values disappears, as does the primary, small magnitude negative lagtime mode.

Scattering signals for individual particles also exhibit significant differences between the RB+DOS and RB+SC cases. For the shortest mixing times, both RB+DOS and RB+SC particles with positive lagtimes exhibit scattering signals similar to that shown in Figure 2a, but for the longest mixing time the scattering signals from RB+DOS particles exhibit two peaks, either one before incandescence and another coincident with incandescence (Figure 2f), or one before incandescence and another after incandescence (Figure 2g), whereas those from RB+SC particles exhibit only one peak.

4.4 Dependence of Lagtime Distributions on SP2 Operating Conditions

Lagtime distributions for RB+SC particles in which laser power and sample flow rate were varied are shown in Figure 4, with laser power increasing from top (2000 mA) to bottom (3000 mA) and sample flow rate increasing from left to right (82, 120, and 240 cm^3 min^{-1}). At the lowest laser power and sample flow rate considered (2000 mA and 82 cm^3 min^{-1}), the lagtimes are predominantly positive (positive-to-negative lagtime ratio 6.1), behavior that would be typically ascribed to a core-shell configuration (Figure 4a). With increasing sample flow rate at this same laser power (Figures 4b and c), the shapes of the lagtime distributions at positive lagtimes remain qualitatively similar, but a mode begins to appear at negative lagtimes concomitant with a decrease in the positive-to-negative lagtime ratio. Likewise, with increasing sample flow rate at a laser power of 3000 mA, the shapes of the lagtime distributions at positive lagtimes are qualitatively similar to each other (Figures 2d–f), with a maximum remaining unchanged near $D_{me, rBC}$ = 290 nm, but there is an increase in the frequency of occurrence of negative lagtimes, which eventually dominate over positive lagtimes. At a given sample flow rate, the lagtime distributions at higher laser power (3000 mA) are qualitatively similar to those at lower laser power (2000 mA), but exhibit large increases in the number of particles with negative lagtimes (and correspondingly large decreases in the positive-to-negative lagtime ratios). The mean values of negative lagtimes are also larger.

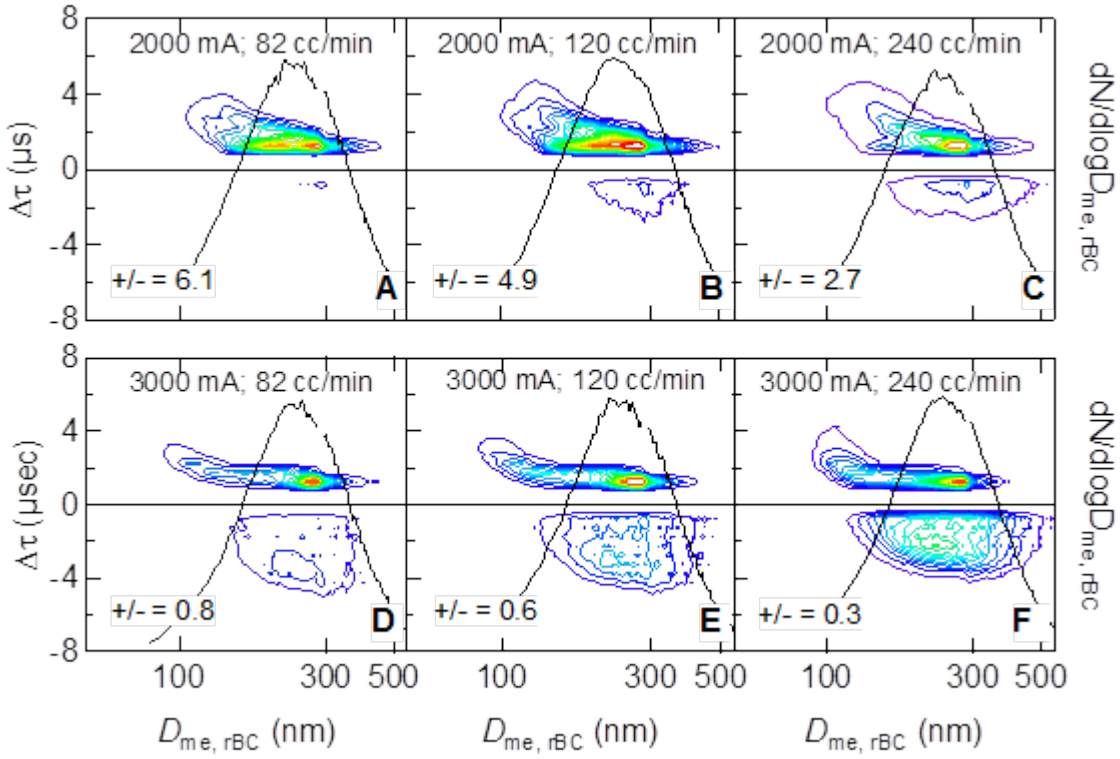

Figure 4. Dependence of RB+SC lagtime distributions on SP2 operating conditions, i.e., sample flow rate (increasing left to right) and injection laser current, which controls laser power (top row: 2000 mA, bottom row: 3000 mA). Also shown are the normalized size distributions of RB-number concentration, $dN_{rBC}/dlogD_{me,\ rBC}$, and the positive-to-negative lagtime ratio (number of particles with positive lagtimes to those with negative lagtimes).

The results of these experiments are also summarized in Figure 5, which encompasses a wider array of conditions than shown in Figure 4. There is a systematic decrease in the positive-to-negative lagtime ratio with either increased laser power or increased sample flow rate, both of which increase particle heating rate. Over the range of SP2 laser powers and sample flow rates examined, the laser power exerts a much larger influence on lagtime distributions than does the sample flow rate.

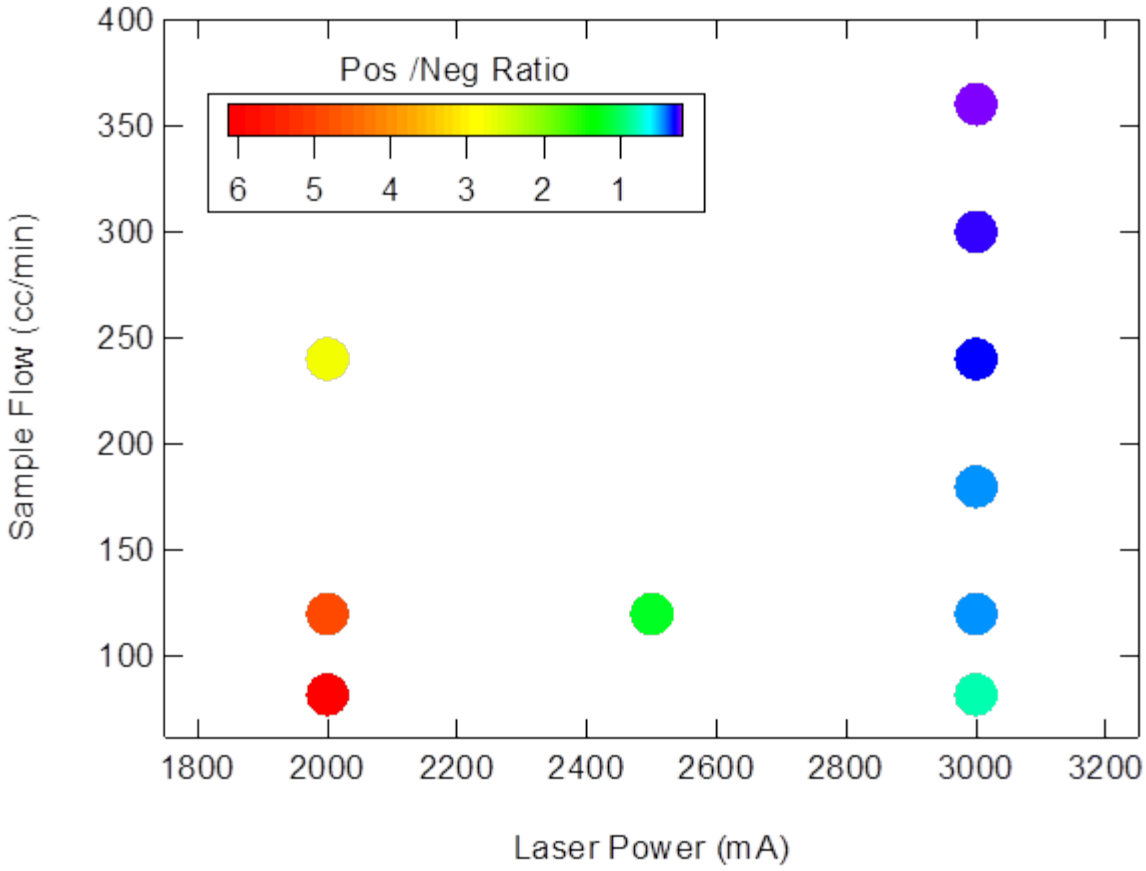

Figure 5. Dependence of positive-to-negative lagtime ratio (number of particles with positive lagtimes to those with negative lagtimes) on SP2 operating conditions, i.e., sample flow rate and injection laser current, which controls laser power.

4.5 Single-Particle Energy Balance in the SP2

The behavior of an rBC-containing particle in the SP2 is determined by both the rate at which the rBC absorbs energy from the laser and the rate at which this energy is dissipated (Moteki and Kondo 2007). This dissipation occurs primarily through conduction to the non-rBC material, from which the energy is subsequently removed through heating and evaporation (i.e., latent heat) of this substance and through conduction to the surrounding gas. The rates of energy absorption and dissipation depend on several factors, the most fundamental of which are the masses and configuration of the rBC and non-rBC components (e.g., core-shell vs. on surface). These determine the absorption cross section and thus the rate at which the particle absorbs incident radiation, and they also govern the rate of intra-particle heat dissipation and the rate of heat conduction to the surrounding gas. This dissipation can be so rapid for particles with a sufficiently small BC mass that these particles never incandesce, and thus will not be detected by the SP2. This effect explains the small particle size limit for SP2 incandescence detection (Schwarz et al. 2010), and it also explains the increased number of lagtimes observed for particles with smaller $D_{me,\,rBC}$ under higher laser power condition (Figure 4, bottom row).

4.6 Lagtimes of Individual Particles

This laboratory investigation explicitly demonstrates that both positive and negative lagtimes can result from particles formed by the coagulation of two solid particles, the coagulation of a solid particle and a liquid droplet, and the condensation of liquid material on a solid particle. Thus, attempts to infer particle morphology from lagtimes alone must be undertaken with extreme caution. In particular, interpretations of lagtime observations based on the assumption of core-shell particle configurations must be regarded with considerable suspicion. In addition, negative lagtimes were observed for each particle type, and accounted for at least 10% of the rBC particles sampled for each experiment, from which it must be concluded that such lagtimes do not correspond to anomalies, but are expected for these and presumably other types of BC- containing particles. For example, Sedlacek et al. (2012) also observed negative lagtimes for ~10% of ambient BC-containing particles under background conditions when biomass burning plumes were not present, and similar values were reported by Moteki et al. (2014) for ambient urban particles. Finally, a substantial fraction of particles in each experiment exhibited scattering signals with two maxima, and as discussed above, such a signal may correspond to either a positive or a negative lagtime, depending on the relative magnitudes of these maxima (Figure 4). As noted above, the magnitudes, and even the sign, of the lagtime are not intrinsic properties of an rBC-containing particle, but rather depend on the rates of energy absorption and dissipation, and thus on SP2 operating conditions.

4.7 Summary

This study demonstrates and highlights several important aspects related to the behavior of rBC-containing particles in the SP2, specifically particle fragmentation, which is important for lagtime analyses and may also be important for other analyses: 1) SP2 operating conditions affect the frequency of particle fragmentation; 2) the physical and chemical properties of rBC-containing particles affect the frequency of fragmentation; and 3) the SP2 appears to fragment a substantial fraction of rBC-containing particles under most operating conditions.

At this point, it is worth examining the utility of lagtimes and lagtime distributions for making inferences about the morphologies and thermochemical properties of rBC-containing particles. From our results, we offer the following observations.

First, two different general lagtime distribution patterns were observed in these experiments: one resulting from coagulation of RB with either solid SC or solid AS, or with liquid DOS at short mixing times, and the other resulting from condensation of liquid DOS onto RB or from coagulation of RB with liquid DOS particles at longer mixing times. These different lagtime distributions are attributed to different particle morphologies. The dependence of the lagtime distribution of coagulated RB+DOS particles on mixing time can be explained by wetting of RB by the DOS, with the lagtime distribution (and the morphology of the particles) changing from being similar to that for RB+SC particles to becoming more similar to that for DOS→RB particles.

Second, this study demonstrates the dominant role played by SP2 operating conditions, specifically laser power and sample flow rate, in determining the observed lagtime distributions. These operating conditions influence the rates of laser heat uptake and internal particle heat transfer (and dissipation) within rBC-containing particles, which in turn affect the fraction of particles that fragment in the SP2 laser and generate negative lagtimes in particular, and the observed lagtime distributions in general. The

effects of operating conditions are shown explicitly for coagulated RB+SC and RB+AS particles and for DOS→RB particles. In all cases, the positive-to-negative lagtime ratio is shown to depend upon these conditions: lower (higher) laser power and lower (higher) sample flow rate generates slower (faster) particle heating and higher (lower) positive-to-negative lagtime ratios. Comparison of lagtime results between different studies with different SP2 instrument parameters will therefore be challenging at best, and to enable meaningful comparisons and to further analyses of SP2 measurements, it is imperative that SP2 laser power and sample flow rate be reported for all future studies. The best practice for quantifying laser power is to measure the scattered light from a standard particle (Schwarz et al. 2010), and the best practice for quantifying particle velocities is to measure the transit times—e.g., full width at half maximum (FWHM)—for non-absorbing particles passing through the laser beam (Schwarz et al. 2015), both of which can be readily accomplished using the same standard particles (e.g., 220-nm PSL).

Third, for given SP2 operating conditions, lagtime distributions also depend on the thermochemical properties of the non-rBC substance. Comparison of lagtime distributions for coagulated RB+SC and RB+AS particles reveals measurable differences in behavior (e.g., RB+AS particles consistently generated higher positive-to-negative lagtime ratios), which are attributed to the greater thermal volatility of AS than that of SC.

Fourth, all particle morphologies and compositions examined here, whether the rBC was on the surface (e.g., RB+SC) or inside the particle (e.g., DOS→RB), exhibited both positive and negative lagtimes. Such a result can confound lagtime-based mixing-state analyses, even those involving examination of individual particle signals. Since positive lagtimes from particles with rBC on the surface can mimic those from particles with core-shell configurations in all aspects, it is not possible to attribute positive lagtimes to a core-shell configuration. Such an attribution could lead to erroneous conclusions, including those regarding radiative properties (especially absorption). The concept of coating thickness for such particles, as is typically obtained from signal scattering and incandescence amplitudes with the implicit assumption of a core-shell configuration, would (of course) be meaningless.

Fifth, the mere presence of a negative lagtime cannot be used to infer particle morphology, because both solid–solid particles and core-shell particles with thick coatings can exhibit negative lagtimes. In this regard, the conclusions of Dahlkötter et al. (2014) that negative lagtimes result only from thickly coated particles in a core-shell configuration is not supported by our observations. The SP2 technique appears to fragment a substantial fraction of rBC-containing particles under most operating conditions, including both ambient conditions and laboratory experiments.

Sixth, although the current results indicate that SP2 lagtime analysis is not able to unambiguously determine particle morphology or to provide information on the thermochemical properties of the non-rBC component directly, the lagtime distribution observations may provide useful information on source attribution and population-based mixing states for rBC-particle populations with different lagtime characteristics. For example, the observations reported by Sedlacek et al. (2012) of two types of rBC-containing particles defined by their lagtime differences, using the same instrument with constant operating conditions, were highly correlated with ambient background particles and tracers of biomass burning transported over the sampling site. In addition, the strong dependence of the magnitudes and signs of lagtimes on SP2 operating conditions might be exploited to probe rBC-containing particles for additional information. For example, the laser power could be modulated for times that would be sufficiently long to yield good statistics but sufficiently short that properties of the aerosol sampled would remain constant.

5.0 Public Outreach

Results obtained from the BC4 study have been disseminated through poster presentations at professional society and DOE meetings.

6.0 BC4 Publications

6.1 Journal Articles/Manuscripts

Sedlacek, AJ, ER Lewis, L Kleinman, J Xu, and Q Zhang. 2012. "Determination of and evidence for non-core-shell structure of particles containing black carbon using the Single-Particle Soot Photometer (SP2)." *Geophysical Research Letters* 39(6), doi:10.1029/2012GL050905.

Sedlacek, AJ, ER Lewis, TB Onasch, AT Lambe, and P Davidovits. 2015. "Investigation of refractory black carbon-containing particle morphologies using the Single-Particle Soot Photometer (SP2)." *Aerosol Science and Technology* 49(10):872-885, doi:10.1080/02786826.2015.1074978.

6.2 Meeting Abstracts/Presentations/Posters

Sedlacek, A, ER Lewis, TB Onasch, AT Lambe, P Davidovits, and L Kleinman. 2013. "Probing rBC-containing particle morphology with a Single-Particle Soot Photometer (SP2)," poster, 4th Atmospheric System Research (ASR) Science Team Meeting, March 2013.

Lewis, ER, AJ Sedlacek, TB Onasch, AT Lambe, and P Davidovits, 2015. "Probing the morphology of black carbon-containing particles," 2015 Gordon Research Conference in Atmospheric Chemistry, Waterville Valley, NH, August 2-7, 2015.

7.0 References

Dahlkötter, F, M Gysel, D Sauer, A Minikin, R Baumann, P Seifert, A Ansmann, M Fromm, C Voigt, and B Weinzierl. 2014. "The Pagami Creek smoke plume after long-range transport to the upper troposphere over Europe–aerosol properties and black carbon mixing state." *Atmospheric Chemistry and Physics* 14: 6111-6137, doi:10.5194/acp-14-6111-2014.

Fuller, KA, WC Malm, and SM Kreidenweis. 1999. "Effects of mixing on extinction by carbonaceous particles." *Journal of Geophysical Research-Atmospheres* 104(D13): 15941-15954, doi:10.1029/1998JD100069.

Moteki, N, and Y Kondo. 2007. "Effects of mixing state on black carbon measurements by laser-induced incandescence." *Aerosol Science and Technology* 41(4): 398–417, doi:10.1080/02786820701199728.

Moteki, N, Y Kondo, and K Adachi. 2014. "Identification by single-particle soot photometer of black carbon particles attached to other particles: Laboratory and ground observations in Tokyo." *Journal of Geophysical Research-Atmospheres* 119(2): 1031-1043, doi:10.1002/2013JD020655.

Schwarz, JP, JR Spackman, RS Gao, AE Perring, E Cross, TB Onasch, A Ahern, W Wrobel, P Davidovits, J Olfert, MK Dubey, C Massoleni, and DW Fahey. 2010. "The detection efficiency of the Single-Particle Soot Photometer." *Aerosol Science and Technology* 44(8): 612-628, doi:10.1080/02786826.2010.481298.

Schwarz, JP, AE Perring, MZ Markovic, RS Gao, S Ohata, J Langridge, D Law, R McLaughlin, and DW Fahey. 2015. "Technique and theoretical approach for quantifying the hygroscopicity of black- carbon-containing aerosol using a Single-Particle Soot Photometer." *Journal of Aerosol Science* 81:110-126. doi:10.1016/j.jaerosci.2014.11.009.

www.arm.gov

U.S. DEPARTMENT OF
ENERGY

Office of Science